Vibrational excitations in thin films studied by spatial dispersion Brillouin spectroscopy

Hua Xia*
Department of Physics and Astronomy, McMaster University, Hamilton, Ontario, Canada L8S 4M1
and National Laboratory of Solid State Microstructures, Nanjing University, Nanjing 210093, China

H. E. Jackson
Department of Physics, University of Cincinnati, Cincinnati, Ohio 45221

K. J. Chen and X. K. Zhang
National Laboratory of Solid State Microstructures, Nanjing University, Nanjing 210093, China

D. Walton
Department of Physics and Astronomy, McMaster University, Hamilton, Ontario, Canada L8S 4M1
(Received 21 February 1996)

By combining a tandem multipass Fabry-Pérot (FP) interferometer with a charge-coupled-device (CCD) imaging detector, we have successfully observed surface Rayleigh waves, longitudinal guided modes, and bulk acoustic modes in dilute magnetic semiconductors, Si- and Ge-based films and superlattices. The inelastically scattered light from acoustic modes is transmitted through the FP off-axis, and is focused on the CCD where it forms concentric rings. We also have demonstrated that the high sensitivity of our system allows the observation of weak bulk acoustic modes from opaque a-Si:H/a-SiN_x:H superlattices.
[S0163-1829(96)10348-9]

I. INTRODUCTION

Acoustic and mechanical properties of thin films and multilayers are usually related to low-frequency vibrational excitations.[1] In the acoustic region, the transverse and longitudinal modes, which always exist in solid materials, are the most prominent excitations. However, the introduction of surfaces and interfaces for single or supported films and multilayers leads to new acoustic excitations with surface characteristics. These excitations consist of shear vertical and longitudinally polarized partial waves whose field components propagate parallel to the surface and decay exponentially with distance into the substrate. For a supported film for which the velocities (v_t^f, v_l^f) of the transverse and longitudinal acoustic waves in the film are less than those (v_t^s, v_l^s) of the substrate, a number of surface acoustic waves in addition to the Rayleigh mode exist. These are called Sezawa and longitudinal guided modes, and their number increases with film thickness. The Sezawa modes exist in the sound-velocity regime bounded by v_t^f and v_t^s. Similarly, the velocities of the longitudinal guided modes are in between v_l^f and v_l^s. Since these frequency regions are separated, the modes are experimentally observable.

Traditional ultrasonic techniques are difficult to use with very thin films; so, Brillouin scattering has become a powerful tool for the characterization of acoustic and mechanical properties of thin films and superlattices.[2–8] In a conventional Brillouin spectroscopy (CBS) system, the observation of the acoustic excitations involves scanning a FP and using a photomultiplier tube (PMT) to record the phonon spectrum.[9,10] Only on-axis light is allowed to contribute to the signal, and only a fraction of the inelastically scattered light is collected, making the CBS inefficient. On the other hand, CCD area detectors[11] are routinely used in Raman instruments to solve this problem, and should accomplish the same purpose in Brillouin spectroscopy.

In reality, spatial dispersion properties of a Fabry-Pérot etalon allow off-axis light to be transmitted in a certain angle range. This means that if the sample is illuminated over a wide area, scattered light of different frequencies forms concentric rings on the focal plane of the detector. Being able to collect all this light at the same time results in a considerable multiplex advantage. Using a CCD area detector we are able to obtain spectra roughly 50 times faster than the scanning method. This has the advantage that the dark count rate of the CCD, which is of the same order as that of a good photomultiplier, has much less time to accumulate, with a corresponding improvement in signal-to-noise ratio. The purpose of this paper is to report the use of a system consisting of a sensitive CCD area detector and a Sandercock tandem FP interferometer in the observation of acoustic excitation spectra. We are referring to this as a spatial dispersion Brillouin spectrometer, or SDBS for short.

This paper is organized as follows. Section II contains a detailed discussion of the optics used for the SDBS. Observation of various acoustic vibrational modes are in Sec. III. Results for several film and multilayer systems are presented: Zn*Y*Se/GaAs, where *Y* stands for Mn, Fe, and Co, crystalline *c*-SiGe alloy, hydrogenated amorphous germanium (*a*-Ge:H) and silicon (*a*-Si:H) films, and *a*-Ge:H/*a*-Si:H and *a*-Si:H/*a*-SiN_x:H superlattices. Through integration processing, the observed two-dimensional acoustic spectral patterns are converted to one-dimensional (1D)

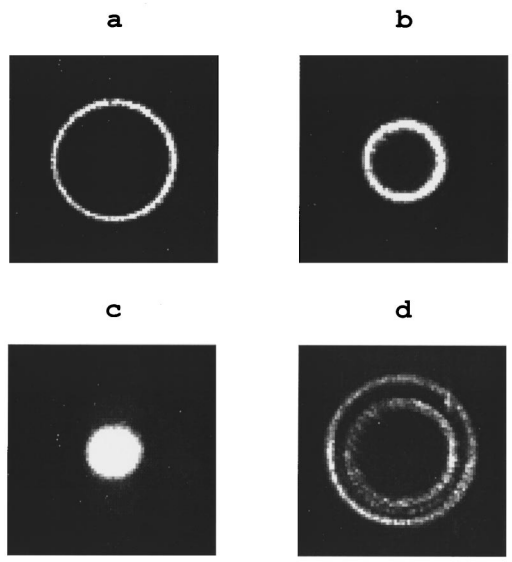

FIG. 1. Two-dimensional spectral patterns of the transmitted elastic light from a *c*-Si film surface, experimentally observed with a 1 sec exposure at a power less than 3 mW. The rings in (a)–(c) correspond to the zero-order elastic peak, while the double rings in (d) come from first-order ''ghost peaks.''

spectra which are similar to those obtained by a conventional scanning method.

II. EXPERIMENT

The experimental setup of the SBDS system was identical to that described in Ref. 13, which consists of a Sandercock tandem 2+2 Fabry-Pérot interferometer (TFPI) and a liquid-nitrogen-cooled 512×512-pixel CCD imaging system. Illumination is provided by the 5145 Å line of an Ar^+ laser. The incident laser beam was defocused with a lens (focus length $f=30$ cm) to cover an area about 200 μm in diameter on the sample. The scattered light is collected by lenses L_1 and L_2 which adjust the beam diameter to match the size of the corner cubes. Since the off-axis scattered light is necessary, the usual pinholes are absent in our system. But two irises, before and after the TFPI, are necessary to eliminate stray light which may contaminate the observed spectra. The polarization of the collected light is chosen through a rotating polarizer. To make the spectral pattern match the chip size on the CCD camera head, another lens with $f=10$ cm is used. In addition, the strong Raman component of the transmitted light is eliminated by using a narrow band filter. And two computers are used to control the TFPI system and the CCD image processing, respectively.

In such a system, the transmitted light of interest will lie between the two bright concentric rings from adjacent orders of elastically scattered light (the tandem feature of the system still allows considerable transmitted intensity of elastic light at higher orders). Since the radius of the ring can be varied by changing the plate spacing of the FP, the strong zero-order elastic ring can be collapsed and only the inelastic light plus the tail of the elastic line is transmitted to form the image pattern, as demonstrated in Fig. 1.

Figures 1(a)–1(c) shows how a zero-order elastic scattering ring is progressively reduced from a narrow ring to a dot and then collapsed from a Si film. After an additional increasing in plate spacing, the first-order ''ghost peaks'' rings are collapsed into the CCD detector, as shown in Fig. 1(d). The first order elastic scattering in a tandem is double peaked because each FP in the tandem transmits at a slightly different plate separation. The phonon rings cannot be seen in Fig. 1 because the elastic light is so strong. In order to collect phonon spectra it is usually necessary to suppress the elastic rings. This is accomplished by adjusting the FP plate separation so that the zero order light is suppressed, and choosing the free spectral range (FSR) so that the radii of the first order ghost peaks are larger than the chip size of the CCD camera head. The experimental system is somewhat unusual, and the optics yields some unexpected benefits. While an initial report has been made in Ref. 12, and a detailed analysis has been presented in Ref. 13, it might be useful to review some important optical parameters here for a better understanding.

A. Maximum frequency range

Since the light contributing to the rings in the pattern is traveling at an angle to the optic axis, the diameter of the ring corresponding to a particular spectral feature, say a phonon, increases along the path. Thus the largest ring that can be transmitted is determined by the diameter of the FP mirrors, and if the FP is multipassed it is limited by the requirement that the different passes do not overlap. If the maximum radius of the transmitted beam after the last pass (limited by the allowable aperture) is a, then the maximum angle is $\tan^{-1}(a/L)$, where L is the total path length from the focus of the lens in front of the first etalon to the outer surface of the second. The difference in frequency, $\Delta\nu_{\max}$, between light transmitted on axis, ν_0, and the light in this ring is independent of the FSR. $\Delta\nu_{\max}$ is calculated in Ref. 13, and the result is

$$\Delta\nu_{\max}\approx\frac{\nu_0}{2}\left(\frac{a}{L}\right)^2. \tag{1}$$

It is obvious that although the FSR, which is determined by the plate separation, can be quite large, no more than $\Delta\nu_{\max}$ can be accessed at any time.

If R is the reflectivity of the FP plates, each pass through the FP will contribute a length $\sim d/(1-R)$ to L. If the number of passes is n_p, and the focal length of the collecting lens in front of the first FP is f, $L\sim[d/(1-R)]n_p+f$. When a tandem is used the distance between the two FP must be added, and L ends up being 50 cm or more. In our system, $a/L\sim 1/50$, and for $\lambda=5145$ Å, the maximum frequency $\Delta\nu_{\max}$ determined by optic geometry is about 120 GHz.

In order to cover a FSR larger than $\Delta\nu_{\max}$, more than one exposure is necessary. However, the multiplex advantage of the instrument is such that an exposure rarely requires more than a few minutes, and this is not a limitation. In fact, we limit the angle through our instrument to less than this to minimize problems caused by walk-off effect of light in between the FP mirrors.

B. Walk-off effect

Since the FP depends on a large number of reflections to achieve transmission, when the light is transmitted at an

angle off axis, the number of reflections is limited by the walk-off of the beam in between the FP plates. A very rough way to estimate this is to assume complete interference as long as they overlap, and none if they do not. With this assumption the maximum angle that can be tolerated before walk-off effect reduces the intensity of the transmitted light to more than 90% of the intensity of the incident beam if it had been transmitted on axis is calculated in Ref. 13 to be

$$\tan\theta \approx \theta \approx -\frac{a(FSR)\ln R}{3c}, \tag{2}$$

where c is the velocity of light. From Eqs. (1) and (2), if ν_0 is the frequency of the transmitted beam at normal incidence to the FP plates, a beam whose frequency is ν will be transmitted at an angle $\cos\theta=(1+\Delta\nu/\nu_0)^{-1}\approx 1-\frac{1}{2}\theta^2$, and

$$\Delta\nu \approx \frac{\nu_0}{2}\left[\frac{a(\mathrm{FSR})\ln R}{3c}\right]^2. \tag{3}$$

It is convenient to express this as a fraction of the FSR:

$$f=\frac{\Delta\nu}{\mathrm{FSR}} \approx \frac{(\mathrm{FSR})(a\ln R)^2}{17.6c\lambda}. \tag{4}$$

With the FSR in GHz, a typical R of 0.93, $r=0.5$ cm, and $\lambda=5145$ Å, we have $f\approx(\mathrm{FSR})/20$.

Thus for a FSR larger than about 25 GHz, a full FSR can be accommodated (subject to the limitation discussed in Sec. II A), but as the FSR is reduced below 25 GHz, less is available. The dependence on the FSR is, of course, due to the increase in plate separation which aggravates the walk-off effect as the FSR is decreased. The light which ''walks off'' can contribute to the background and reduce the contrast, and for applications where a low background is essential the maximum acceptance angle should be reduced even further. This can be accomplished by placing an iris at the exit of the last FP.

C. SDBS finesse

Since no pinholes are employed, the finesse of the SDBS system is determined by the reflectivity and flatness of the FP plates. According to Born and Wolf,[14] the reflectivity finesse of a single pass FP is

$$f_r=\frac{\pi\sqrt{R}}{(1-R)}. \tag{5}$$

This expressions assumes perfect FP plates. For real plates a plate flatness finesse, $M/2$, can be specified if the flatness is λ/M, and the final finesse becomes

$$f^{-1}=\sqrt{\left(\frac{2}{M}\right)^2+\left(\frac{1}{f_r}\right)^2}. \tag{6}$$

For a multipass instrument, if the number of passes is n_p, the finesse becomes

$$F=\frac{f}{\sqrt{(2^{1/n_p}-1)}}. \tag{7}$$

The width of the ring recorded by the detector is proportional to $\delta\nu_f=F\nu_0$, and $\delta\nu_f$ is the width of the spectral feature recovered upon deconvolution. This will be *narrower* than that obtained with a scanning instrument using the same number of passes and the same FSR because the scanning instrument must use pinholes to limit the divergence of the beam, and the ''pinhole finesse'' decreases the instrumental resolution (which, of course, would be virtually unusable without pinholes). Thus the finesse with an area detector can be expected to be equal to or higher than that of the scanning configuration. It may appear paradoxical that removing the pinholes results in a higher finesse. In order to understand this result it should be noted that when scanning the light collected on axis corresponds to the FP plate separation, and if no pinholes are used, light of longer wavelength can be transmitted at an angle which is only limited by walk off. Light transmitted at an angle will be attenuated by a factor of 2 when the number of reflections p is at least $p=\ln(1-\sqrt{0.5})/\ln R$, which for a typical reflectivity of 0.93 yields $p\geqslant 17$. If the radius of the beam is a, and the plate separation is d, the angle between this ray and the central beam is $\alpha=\tan^{-1}(a/17d)\approx a/17d$.

On the other hand, the change in angle θ corresponding to a change of π (corresponding to increasing the order by 1) in the phase factor δ is $\Delta=\sin^{-1}(\lambda/d)\approx\lambda/d$, which is much less than α, and many orders can be transmitted. This will result in a broad elastic tail unless pinholes are used to limit the beam divergence.

D. Ring width and intensity distribution

From Eq. (1) a ring of radius a on the detector corresponds to a frequency difference $\Delta\nu=\nu-\nu_0$ such that

$$\Delta\nu \approx Aa^2, \tag{8}$$

where A is constant determined by the optical parameters of the system. If the width of this ring on the detector is δa, it originates from a corresponding ring of radius s and width δs on the sample. The width is determined by the finesse of the two FP's, and if the bandpass is $\delta\nu_f$, the width δa on the detector is

$$\delta a=\frac{\partial a}{\partial\nu}\delta\nu_f=\frac{\delta\nu_f}{2Aa}=\frac{C}{a}, \tag{9}$$

where $C=\delta\nu_f/2A$ is a constant. Thus the light corresponding to the frequency range $\nu\pm\delta\nu_f$ is displayed over a band $a\pm C/a$. It comes from a corresponding band $s\pm C'/s$ on the sample. This means that the changes in the ring radius and its width are directly correlative to a proportional space scanning on sample surface. If the sample is uniformly illuminated with monochromatic light, the radius of the ring recorded by an area detector can be changed by changing the plate separation of the FP. Although the increase in width of the ring is balanced by a decrease of ring radius, the integrated intensity on the detector is independent of the size of the ring.

However, because of the drop off in intensity of the laser beam it is impossible to obtain uniform illumination. For a Gaussian laser intensity profile, the irradiance is

$$I(r)=\frac{P}{\pi w^2}e^{-r^2/w^2}, \tag{10}$$

where P is the total power in the beam, and w is the width of the beam. The exponential drop off in the intensity on the sample surface will produce a corresponding exponential drop off on the detector, and a consequent weakening of the signal. In order to maximize the signal it is best to adjust the plate separation so that the inelastic light of interest is as close to the center of the ring pattern as possible. If the second order elastic ring appears, and must be suppressed, this can be accomplished with an iris.

Unfortunately the nonuniform illumination complicates the determination of absolute, or even relative scattering intensities. In principle they could be determined by calibrating the system by measuring the intensity of the elastic light as the corresponding ring size is changed. In practice, because the sample contains inhomogeneities, we have found it difficult to obtain consistent results. In any case, the intensity of a spectral feature has not been of interest in our investigations, and a solution to this problem has not been sought with sufficient dedication.

E. Phase velocity of acoustic excitations

In our experiments a quasibackscattering geometry is used. The in-plane wave vector component for surface acoustic excitations is linked to the wave vector k_0 of incident radiation by the expression $q=k_0(\sin\theta_i+\sin\theta_s)$, where θ_i and θ_s are the incident and scattered angles normal to the surface. The phase velocity of the surface acoustic modes can be deduced from

$$v_{\rm surf}=\nu_{\rm surf}/k_0(\sin\theta_i+\sin\theta_s), \tag{11}$$

where $\nu_{\rm surf}$ is the measured frequency shift. But for bulk vibrational excitations, the phase velocity is calculated from the measured frequency ν_B as follows:

$$v_{\rm TA,LA}=\nu_B/2nk_0, \tag{12}$$

where n is the refractive index of the material. In our experiments the in-plane wave vector component was chosen along the [100]- and [110]-axis of lattice (001) planes.

III. RESULTS AND DISCUSSION

A. Vibrational spectra in transparent films

It is well-known that the low-frequency vibrational spectra of a supported film depend strongly on the thickness of the film under investigation. When the thickness h is comparable to the phonon wavelength, discrete guided longitudinal and transverse acoustic modes are present in the spectrum, whose number increases with qh. For thicker films, these modes will form continuous spectra which extend to the higher frequencies of the bulk phonons in the substrate. Using our spatial dispersion Brillouin spectrometer, these surface and bulk acoustic excitations can be observed by choosing an appropriate FSR and ring radius.

The dilute magnetic semiconductor ZnYSe/GaAs (Y=Mn, Fe, or Co) system is a semi-transparent heterostructure. Owing to the phase velocities of longitudinal and transverse acoustic modes in the films being less than those of GaAs substrate, this structure shows very rich vibrational spectra as illustrated in Fig. 2 from a ZnFeSe/GaAs sample. The two-dimensional (2D) spectral pattern in Fig. 2(a) shows two dim inner rings due to phonons and bright outer rings due to first-order transmitted elastic peaks, i.e., ghost peaks, where a FSR of 24.6 GHz is used. The innermost ring with a frequency shift of 8.5 GHz is due to the surface Rayleigh wave (RW), propagating along the air-film interface. The phonon mode at 16.8 GHz, associated with the other inner ring, shows a strongly wave-vector-dependent frequency shift. However, similar to the RW, its phase velocity is nearly a constant. The calculated velocity is very close to the longitudinal sound velocity of ZnSe film. As previously found in the ZnSe/GaAs by Hillebrands *et al.*,[3] this mode should be the longitudinal counterpart to the Rayleigh wave, i.e., the longitudinal guided mode (LGM), with a phase velocity slightly below the longitudinal sound velocity. The so-called LGM is also observed as an inner ring in Fig. 2(b), where a 72.9 GHz FSR is used. The outer ring as well as the ring in Fig. 2(d) are the phonon of transverse acoustic (TA) modes with a frequency shift of about 26.8 GHz. In addition, the longitudinal acoustic (LA) mode is also observed at a frequency of about 49 GHz. All the data were taken with a 2.5-min exposure, but the scattering intensity of each mode is very different.

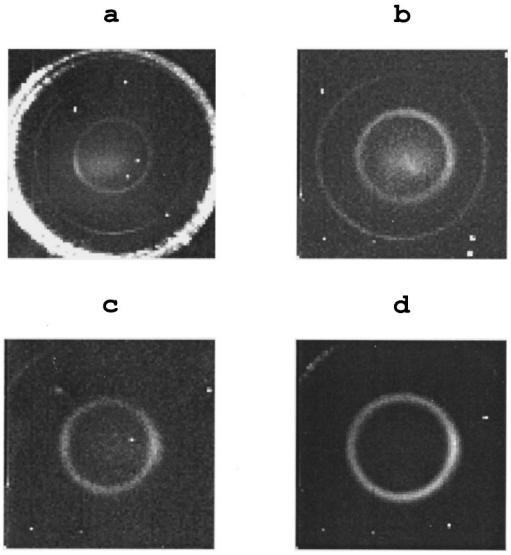

FIG. 2. Two-dimensional phonon modes of the surface Rayleigh wave, longitudinal guided acoustic wave, transverse and longitudinal acoustic waves from dilute magnetic semiconductor ZnFeSe/GaAs heterostructures, where data are read out in a bin of 6×6 pixels and 2.5 min.

Figure 3 shows the three-dimensional (3D) spectral patterns, which correspond to the LGM and TA modes in Fig. 2(b) and to the LA mode in Fig. 2(d). Here a bin of 6×6 pixels was used and the data in the CCD chip are read out in a dimension of 85×85 bins. The high scattering intensity from the LA mode, compared with the intensity of the LGM in Fig. 3(a), should be associated with a large elasto-optic coefficient. We note that due to larger film thickness (h=1.5 μm), the higher-order Sezawa waves and longitudinal guided modes cannot be distinguished from the background in our samples. Since the phase velocity of the LGM in the

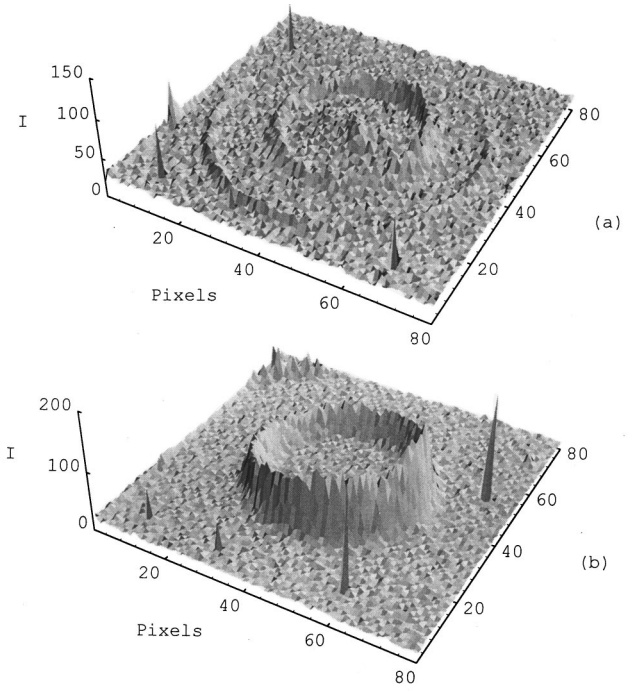

FIG. 3. Three-dimensional phonon structures of (a) the longitudinal guided mode, transverse acoustic modes in Fig. 2(b), and (b) longitudinal acoustic modes in Fig. 2(d). The discrete small peaks are due to cosmic rays.

films can be obtained using Eq. (11), this allows us to evaluate the variation and dependence of the elastic properties on doping concentration and ion radius, as illustrated in Fig. 4. The results clearly show that the elastic constants increase with both increasing doping concentration and increasing ion radius or atomic number.

B. Vibrational spectra in opaque films and superlattices

For opaque semiconductors, the surface ripple effect is the dominant mechanism for Brillouin scattering. Thermally

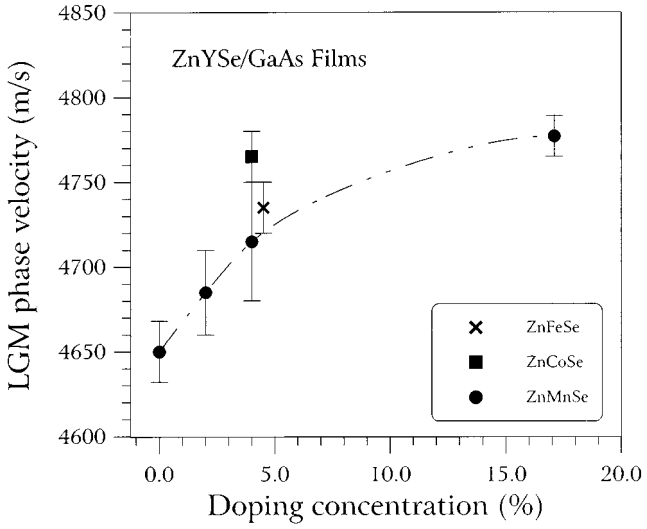

FIG. 4. Dependence of phase velocity of the LGM on doping concentration in ZnYSe/GaAs (Y=Fe, Co, and Mn) heterostructures.

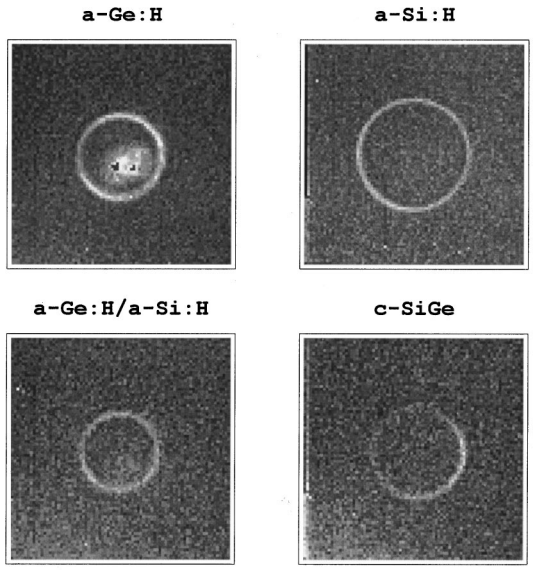

FIG. 5. Two-dimensional phonon spectra of surface Rayleigh wave from hydrogenated amorphous germanium (a-Ge:H) and silicon (a-Si:H) films, a-Ge:H/a-Si:H superlattice, and c-SiGe alloy. The spectra were observed with a power of 100 mW and at incident angles of 75° for a-Ge:H and c-SiGe, 80° for a-Si:H, and 85° for a superlattice. The angle between incident and scattered light is 15°.

excited acoustic modes, which corrugate the nominal plane surface, produce a small cross section for inelastic scattering. Experimentally, the phonon spectra measurements we have performed are sufficiently sensitive to such a small cross section.

Figure 5 displays the phonon spectra of a surface Rayleigh wave (RW) from hydrogenated amorphous germanium (a-Ge:H) and silicon (a-Si:H), a-Ge:H/a-Si:H superlattice (SL), and crystalline silicon germanium (c-SiGe) alloy in which the germanium content is 2.3%. Their frequency shifts are found at 9.4, 13.8, 17.5, and 12.3 GHz, respectively, where the angle θ_i of incidence of light is 75° for a-Ge:H and c-SiGe films, 80° for a-Si:H film, and 85° for a-Ge:H/a-Si:H SL. 1D spectra were obtained by summing over bins at the same radius, as shown in Fig. 6. We found that even though the average intensity in each pixel may only be a few counts, the integrated spectrum may have a few hundred counts with a good signal-to-noise ratio. Of course, phonon spectra are easily contaminated by stronger elastic Rayleigh wing scattering due to inhomogeneity in the sample surface. In order to avoid this, these spectra were taken in an appropriate ring radius which is determined by FP plate separation. Based on the incident and scattered angles used here and Eq. (11), the phase velocities of the Rayleigh waves are found to be 2620, 3720, and 3260 m/s for a-Ge:H, a-Si:H films and for a-Ge:H/a-Si:H SL, respectively. The phase velocity (v_R=4850 m/s) of c-GeSi film is about 1% lower than that of crystalline silicon due to 2.3% Ge concentration.

Although the appearance of the phonon spectrum from a-Ge:H film is different from our previous work[15] due to film thickness, the measured phase velocity in both cases is very close. For a-Si:H films, our measured velocity is smaller than that reported in Ref. 16. This can be attributed to the influence of hydrogen concentration which causes dy-

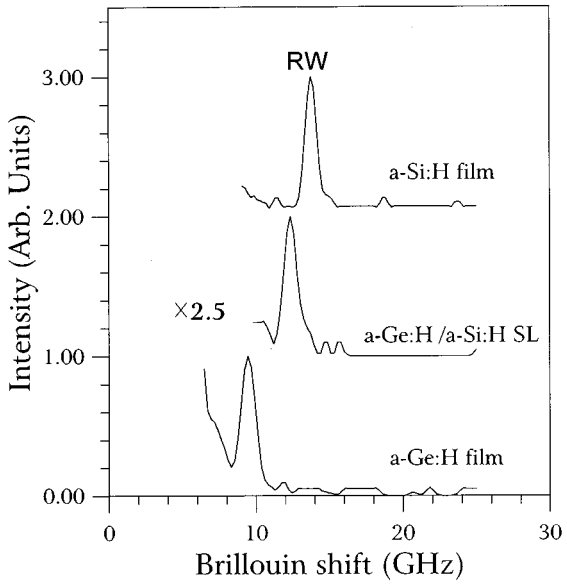

FIG. 6. 1D phonon spectra from surface Rayleigh waves (RW), converted from Fig. 5, where the spectral intensities are normalized with a magnification of 2.5 times for a-Ge:H/a-Si:H SL.

namical properties of the film to soften with increasing hydrogen content. In the case of a superlattice, since the modulation period (Λ) is much less than the phonon wavelength ($\sim$ 3000 Å), its physical properties also can be described by an effectively homogeneous film of thickness h. It follows that the phase velocity of a surface Rayleigh wave in a-Ge:H/a-Si:H SL can be characterized by the corresponding quantities in the constituents:[16]

$$v_R=\Lambda\left\{\left(\frac{d_A}{v_R^A}\right)^2+\left(\frac{d_B}{v_R^B}\right)^2+\frac{d_Ad_B}{v_R^Av_R^B}\left(\frac{\rho^Av_R^A}{\rho^Bv_R^B}+\frac{\rho^Bv_R^B}{\rho^Av_R^A}\right)\right\}^{-1/2}, \tag{13}$$

where A and B represent a-Ge:H and a-Si:H films, $d_A=d_B=50$ Å, $\Lambda=100$ Å, $\rho^{a\text{-Ge:H}}=5.05$ g/cm^3, and $\rho^{a\text{-Si:H}}=2.21$ g/cm^3, respectively. Substituting these values into the above equation, the calculated phase velocity (3170 m/s) is consistent within 3% with the measured velocity. Note that the above calculation does not include any influence from the substrate because the thicknesses of our samples are greater than one phonon wavelength. It is reasonable to ignore the effect of the substrate on the phonon spectrum.

Finally we wish to illustrate the high sensitivity of our system: although the surface Rayleigh wave can be observed, the vibrational spectra of bulk acoustic modes from a-Si:H/a-SiN$_x$:H quasiperiodic superlattices (QSL) are too weak to be observed after scanning for two hours with a high contrast and good finesse 3+3 TFPI. In fact, the insulator layers in the superlattice cause a dielectric fluctuation much smaller than that in semiconductor layers. Thus, the small cross section due to small dielectric fluctuation in a-SiN$_x$:H and opacity in a-Si:H makes it difficult to observe bulk vibrational modes.[17] However, using our Brillouin spectroscopy, we have successfully observed longitudinal acoustic modes with a 5 min exposure. A 1D phonon spectrum obtained by scanning a 3+3 tandem FP is shown in Fig. 7(a). 2D and 1D phonon spectra obtained using our system are demonstrated in Fig. 7(b). Although the peak is seriously broadened, a good line shape and signal-to-noise ratio can be found. However, this mode cannot be seen in Fig. 7(a) at all.

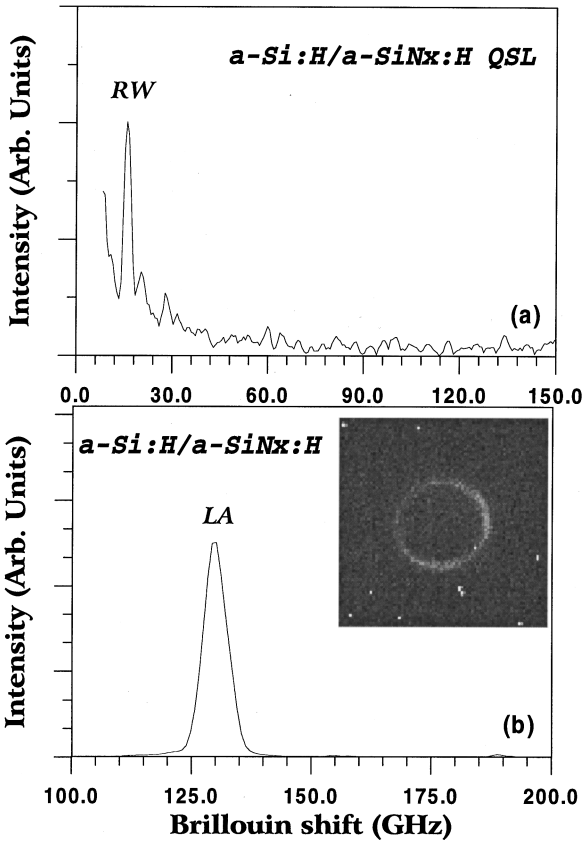

FIG. 7. Phonon spectra observed using (a) the conventional Brillouin spectrometer, and (b) using our spatial dispersion Brillouin spectrometer on an a-Si:H/a-SiN$_x$:H quasiperiodic superlattice (Ref. 17).

IV. CONCLUSION

In conclusion, the measurements on acoustic excitations have been carried out to characterize the vibrational properties of ZnYSe/GaAs (Y=Mn, Fe, and Co) heterostructures, Si- and Ge-based films, as well as superlattices by means of a newly designed Brillouin spectrometer, which combines a highly sensitive CCD camera detector and a tandem Fabry-Pérot interferometer. In contrast with a conventional Brillouin spectrometer using a scanning method, we have demonstrated that three- and two-dimensional phonon spectral patterns can be observed within a short time. Despite the fact that no pinholes are used, this system has shown high sensitivity on a weak phonon signal, and tolerable finesse and contrast.

Furthermore, the observation of phonon modes in 2D and 3D might offer another possibility to do direct space resolved measurements or scanning of the sample surface as in micro-Raman imaging spectroscopy. This potential application may

provide more information related to the spatially distributed scattering intensity, phonon frequency, and spectral width at the locations at which the spectra are taken. It should be noted that inhomogeneities on the sample surface or subsurface actually may result in variations of these parameters, and would become an observable effect with our instrument.

ACKNOWLEDGMENTS

The authors appreciate the contributions of Dr. Z. F. Li for sample preparation. This research is supported by the Natural Sciences and Engineering Research Council of Canada, the National and Jiangsu Provincial Natural Science Foundations of China, and in part by NSF and ARO (H.E.J.).

*Author to whom correspondence should be addressed. Department of Physics, Colorado State University, Fort Collins, Colorado 80523. Electronic address: huax@lamar.colostate.edu

[1] G. W. Farnell and E. L. Adler, in *Physical Acoustics*, edited by W. P. Mason and R. N. Thurston (Academic, New York, 1972), Vol. 9, p. 35.

[2] I. G. Siny, C.-S. Tu, and V. H. Schmidt, Phys. Rev. B **51**, 5659 (1995).

[3] B. Hillebrands, S. Lee, G. I. Stegeman, H. Cheng, J. E. Potts, and F. Nizzoli, Phys. Rev. Lett. **60**, 832 (1988).

[4] Hua Xia, X. K. Zhang, An Hu, S. S. Jiang, R. W. Peng, Wei Zhang, Duan Feng, G. Carlotti, D. Fioretto, and G. Socino, Phys. Rev. B **47**, 3890 (1993).

[5] Hua Xia, X. K. Zhang, X. X. Qu, Wei Zhang, X. Y. Qu, Duan Feng, and J. Y. Wang, Phys. Rev. B **45**, 5140 (1992).

[6] F. Nizzoli, C. Byloos, L. Giovannini, C. E. Bottani, G. Ghislotti, and P. Mutti, Phys. Rev. B **50**, 2027 (1994).

[7] L. Bassoli, F. Nizzoli, and J. R. Sandercock, Phys. Rev. B **34**, 1296 (1986).

[8] G. Ghislotti, and C. E. Bottani, Phys. Rev. B **50**, 12 131 (1994).

[9] J. R. Sandercock, Solid State Commun. **26**, 547 (1978).

[10] J. R. Sandercock, in *Light Scattering in Solids III*, edited by M. Cardona and G. Güntherodt (Springer, Berlin, 1982), p. 173.

[11] James C. Tsang, *Light Scattering in Solids V*, edited by M. Cardona and G. Güntherodt (Springer-Verlag, Berlin, 1989), p. 255.

[12] D. Walton, J. J. Vanderwal, and P. Zhao, Appl. Spectrosc. **46**, 373 (1992).

[13] D. Walton, J. J. Vanderwal, H. Xia, and P. Zhao, Rev. Sci. Instrum. **67**, 2727 (1996).

[14] M. Born and E. Wolf, *Principles of Optics* (Pergamon, New York, 1970), p. 360.

[15] Hua Xia, J. G. Jiang, Wei Zhang, K. J. Chen, X. K. Zhang, G. Carlotti, D. Fioretto, and G. Socino, Solid State Commun. **84**, 987 (1992).

[16] Hua Xia, G. Carlotti, G. Socino, K. J. Chen, Wei Zhang, Z. F. Li, and X. K. Zhang, J. Appl. Phys. **75**, 475 (1994).

[17] Hua Xia, X. K. Zhang, K. J. Chen, G. X. Cheng, D. Feng, G. Socino, L. Palmieri, G. Carlotti, D. Fioretto, and F. Nizzoli, Phys. Rev. B **42**, 11 288 (1990).